LIMNOLOGY and OCEANOGRAPHY

ASLO

Limnol. Oceanogr. 69, 2024, 246–261

doi: 10.1002/lno.12471

Seasonal and spatial variability of CO_2 emissions in a large tropical mangrove-dominated delta

Raisa S.A. Chielle [1], **Rozane V. Marins** [1*], **Mariany S. Cavalcante** [1], **Luiz C. Cotovicz Jr** [1,a]
Institute of Marine Sciences (LABOMAR), Federal University of Ceará (UFC), Fortaleza, Brazil

Abstract

This study quantified the seasonal and spatial variability of partial pressure of CO_2 (pCO_2) and water-atmosphere CO_2 fluxes in the Parnaíba River Delta, the largest delta in the Americas. It is a pristine equatorial, mangrove-dominated environment located in a transitional between humid and semi-arid climates, with marked seasonality in rainfall and river discharge. Major channels and bays were sampled during dry and wet seasons, with continuous measurements of pCO_2, temperature, salinity, and wind velocity. Subsurface water samples were collected in discrete stations for pH, total alkalinity (TA), dissolved inorganic carbon (DIC), dissolved oxygen and chlorophyll *a* quantification. A significant positive correlation between carbonate system parameters with salinity was found in both periods, with salinity significantly higher in the dry season. Strong deviations of pCO_2, TA, and DIC from two endmembers conservative mixing were found, particularly in mangrove-dominated waters, due to organic matter degradation. The Delta showed high spatial variability of pCO_2, with the highest values in mangrove-dominated waters, moderate in the river-dominated regions, and lowest in the high salinity areas, suggesting that pCO_2 variability is likely controlled by a combination of river-ocean mixing and biological processes (respiration and photosynthesis). The Delta outgasses about 20 times less CO_2 in the dry season (9.06 ± 11.09 mmol $m^{-2}.d^{-1}$) than in the rainy season (209.68 ± 250.87 mmol m^{-2} d^{-1}). Our results indicate this large mangrove-dominated tropical delta is an important source of CO_2 to the atmosphere, but a sharp decrease was observed during dry periods.

Although corresponding to only 7% of the total area of the global ocean, the coastal ocean is a highly active biogeochemical area where several processes and transformations of carbon occur (Gattuso et al. 1998), especially in the estuarine zone (McLusky and Wolanski 2011; Bauer et al. 2013). The estuaries, in their different typologies, are defined as transitional areas between the riverine domain and marine waters, receiving significant inputs of organic and inorganic carbon from different sources, such as rivers, groundwater, mangrove tidal creeks, and the ocean (Abril and Borges 2005; Cole et al. 2007; Cai 2011; Dürr et al. 2011; Bauer et al. 2013; Chen et al. 2018).

A delta is a coastal estuarine environment created by the deposition of riverine sediments to the coastline more rapidly than its removal and/or redistribution by tides or waves (Bianchi 2007). These environments are mostly sources of CO_2 to the atmosphere (Laruelle et al. 2013), mainly due to the intense oxidation of the organic matter carried out from rivers and the input of CO_2-enriched freshwaters, porewaters, and groundwaters (Gattuso et al. 1998; Borges and Abril 2010; Chen et al. 2018; Call et al. 2019). The river flow is a major driver of biogeochemistry dynamics in deltas (Paula Filho et al. 2020), and its mixture with seawater creates estuarine conditions, establishing hotspots of carbon modifications (Bouillon et al. 2005; Borges et al. 2018; Maier et al. 2021). In addition, the close connection of deltaic systems to wetlands, such as mangrove forests, has the potential to increase its CO_2 emissions (Bouillon et al. 2005).

The latest global estimate shows estuaries and deltas as significant sources of CO_2 into the atmosphere, with a flux of 0.1 Pg C yr^{-1} (Chen et al. 2013). This study indicated that the environments located at tropical latitudes usually present the largest fluxes per unit area. However, these estimates still have large uncertainties, mainly due to their great spatial and seasonal variability. Furthermore, tropical estuaries are

*Correspondence: rmarins@ufc.br

Additional Supporting Information may be found in the online version of this article.

[a]Present address: Department of Marine Chemistry, Leibniz Institute for Baltic Sea Research (IOW), Rostock, Germany

Author Contribution Statement: R.S.A.C. performed formal analysis, investigation, and writing–original draft. R.V.M. performed conceptualization, resources, writing–review and editing, project administration, and funding acquisition. M.S.C. performed formal analysis and investigation. L.C.C. performed investigation and interpretation of data.

still under sampled compared to subtropical and temperate ecosystems. Most of the largest rivers in the world regarding water discharge are in the tropics (Latrubesse et al. 2005), and, thus, these tropical estuaries and deltas are an important component in the transport of carbon to the open ocean and in the emissions of CO_2 to the atmosphere.

Mangroves are one of the most productive ecosystems in the world, storing and sequestering large amounts of carbon in their biomass and soils (Bouillon et al. 2008; Alongi 2012). Although the whole system is an important carbon sink, most mangrove tidal creeks, as well as the adjacent waters act as a strong source of CO_2 to the atmosphere (Borges et al. 2003). This high CO_2 flux is usually attributed to the exchanges with porewater enriched in pCO_2, dissolved inorganic carbon (DIC) and total alkalinity (TA) (Call et al. 2019); and the metabolic activity in sediments which produce TA and DIC through different diagenetic pathways (Sippo et al. 2016). Therefore, compared to the rivers, the surface waters of mangrove creeks are normally enriched in TA and DIC, and the ratios between DIC and TA can provide important insights into the CO_2 dynamics of these coastal systems (Sippo et al. 2016).

The latest global assessment of CO_2 efflux in mangrove-dominated estuaries estimated emissions on the order of 34.1 ± 5.4 Tg C per year (Rosentreter et al. 2018*a*). However, only one Brazilian system was included in this compilation. The lack of data from Brazilian estuarine and deltaic systems in adequate spatial and seasonal resolution is the main reason these systems remain out of global estimates.

With about 10,000 km^2 of mangrove forests, Brazil is the third country in the mangrove area, containing roughly 7.1% of the total global area (Magris and Barreto 2010). Most of the mangrove area in Brazil is concentrated in the Northern equatorial region (60%–70%), and one of the largest areas is the Parnaíba River Delta (PRD). The PRD is a wave-dominated and tidally influenced delta, the largest open sea delta in the Americas, containing a complex system of islands, multiple tidal channels, and fluvial-marine plains which harbor around 1500 km^2 of mangrove forests (Lacerda 2018). The PRD is considered an almost pristine environment, with little industrial development, and ecotourism and agriculture as the main economic activities. The first research about CO_2 dynamics in PRD assessed the main channel of the river and only two creeks, during the rainy season (Chielle et al. 2023). However, due to the complexity of the PRD, it was essential to extend the sampling to other channels and bays of the delta and to access the seasonal variability, in order to understand the heterogeneity of the PRD and the extension of the estuarine region over the marine intrusion influence.

As a protected area, the delta is a key environment in understanding the carbon cycle in natural environments, and how climate change may influence its dynamics. We hypothesize that due to the high variability of river discharge and precipitation, the delta will present marked seasonal variability of pCO_2 values and fluxes, as well as a strong spatial heterogeneity in the processes that control these fluxes.

Methods

Study area

The PRD is located on the northeastern equatorial Brazilian coast (41°10′W–42°20′W; 03°10′S–02°45′S), between the states of Ceará, Piauí, and Maranhão. The PRD is formed by a complex system with more than 70 islands, multiple tidal channels, and fluvial-marine plains colonized by mangrove forests with trees reaching 20 m, and many migrating coastal dunes (Lacerda 2018). In 1996, the delta was included in an Environment Protection Area (EPA) (MMA 2006), due to its great biodiversity and ecological importance in fauna and flora. The establishment of the EPA and the low population density of the area characterize the ecosystem as an almost pristine environment, with small industrial development, and small harbors to attend ecotourism, agriculture, and fishing.

The delta is situated on a climatic transitional coast, between the NE semi-arid and Amazon humid climate, mainly influenced by the Intertropical Convergence Zone (ITCZ) and the South Atlantic anticyclone. There are two marked seasons (Supporting Information Fig. S1): a rainy period from January to May–June (monthly average = 181 mm) with maximum precipitation usually happening in April (267.2 mm); and a dry period from July–August to December (monthly average: 28.5 mm). The river discharge follows the pattern of the precipitation, generally higher in April (1460 $m^3\ s^{-1}$). However, the discharge is also regulated by the Boa Esperança reservoir (around 700 km upstream from the Parnaíba river mouth), and it is never below 100 $m^3\ s^{-1}$ even under very dry conditions. The delta is classified as a wave-dominated asymmetric delta, due to its outline and spits west of the river mouth (da Silva et al. 2015). The tide is semidiurnal, reaching amplitudes of 3.3 m during spring tide while it reaches only 1.7 m during neap tide (mesotides) (da Silva et al. 2015).

Sampling strategy

The PRD includes the Parnaíba River, Caju, Melancieiras, and Tutóia Bays together with other tidal channels. The sampling campaigns occurred in March 2018, the rainy season, and in December 2019 and December 2021, the dry season (Fig. 1). Continuous, real-time measurements of pCO_2, temperature, salinity, and wind velocity were taken by an underway CO_2 equipment coupled with a thermosalinograph and an anemometer. Subsurface water samples were collected in discrete stations for pH, TA, DIC, dissolved oxygen (DO), and chlorophyll *a* (Chl *a*) analysis (Fig. 1). DO and pH were measured in situ using a multiparametric probe (YSI® Professional Plus) and a Methrom® portable electrode in the NBS scale, respectively. Due to a malfunctioning of the electrode, there is no pH data from the December 2021 campaign.

Continuous measurements

Surface water temperature and salinity were measured by a thermosalinograph (SeaBird Electronics®), while wind speed and direction were measured by an anemometer (Davis® S-WCF-M003) attached to the vessel. Wind speed and direction were rectified using vector decomposition.

The pCO_2 in estuarine water and atmosphere was measured using a semi-autonomous underway equipment. Detailed descriptions of this equipment can be found in previous studies conducted in estuarine and continental shelf waters (Pierrot et al. 2009; Carvalho et al. 2017; Cotovicz et al. 2020*a*; Chielle et al. 2023). In summary, a flux of subsurface estuarine water is pumped to the equilibrators. After the equilibrium with the water, the air is dried and passes through a non-dispersive infrared analyzer (NDIR Li-Cor® Li-7000, USA) to measure its CO_2 concentration as the molar fraction of CO_2 (xCO_2^{eq}). The system, then, calculates the partial pressure of CO_2 (in μatm) from the molar fraction of CO_2 in dry air (μatm) considering surface water temperature and 100% saturation of water vapor, according to (Weiss and Price 1980):

$$pCO_2^{eq} = XCO_2^{eq*}\left(P_{eq} - P_w^{eq}\right), \quad (1)$$

where P_{eq} is the barometric pressure at equilibrium and P_w^{eq} is the water vapor pressure (in atm) calculated at the equilibrator temperature.

A temperature correction was applied to convert the pCO_2 (μatm) measured in the equilibrator (pCO_2^{eq}) to the pCO_2 at in situ surface water temperature conditions (pCO_2^{sw}) (Takahashi et al. 2002):

$$pCO_2^{sw} = pCO_2^{eq*} \exp^{[0.0423*SWT-Teq]} \quad (2)$$

Manual calibration is completed before starting the measurements using certified standards (360, 1009, and 2009 ppmv, White Martins Certified Material). After, every 6 h the system runs an automated calibration. Nitrogen gas is used as zero, free from CO_2 and water vapor. The precision of pCO_2 measurements was around ± 2 ppmv verified periodically using these certified gas standards.

Laboratory analysis

Water samples for determination of TA were collected in duplicate using 500 mL borosilicate bottles. To preserve the samples, we added 200 μL of a saturated solution of $HgCl_2$,

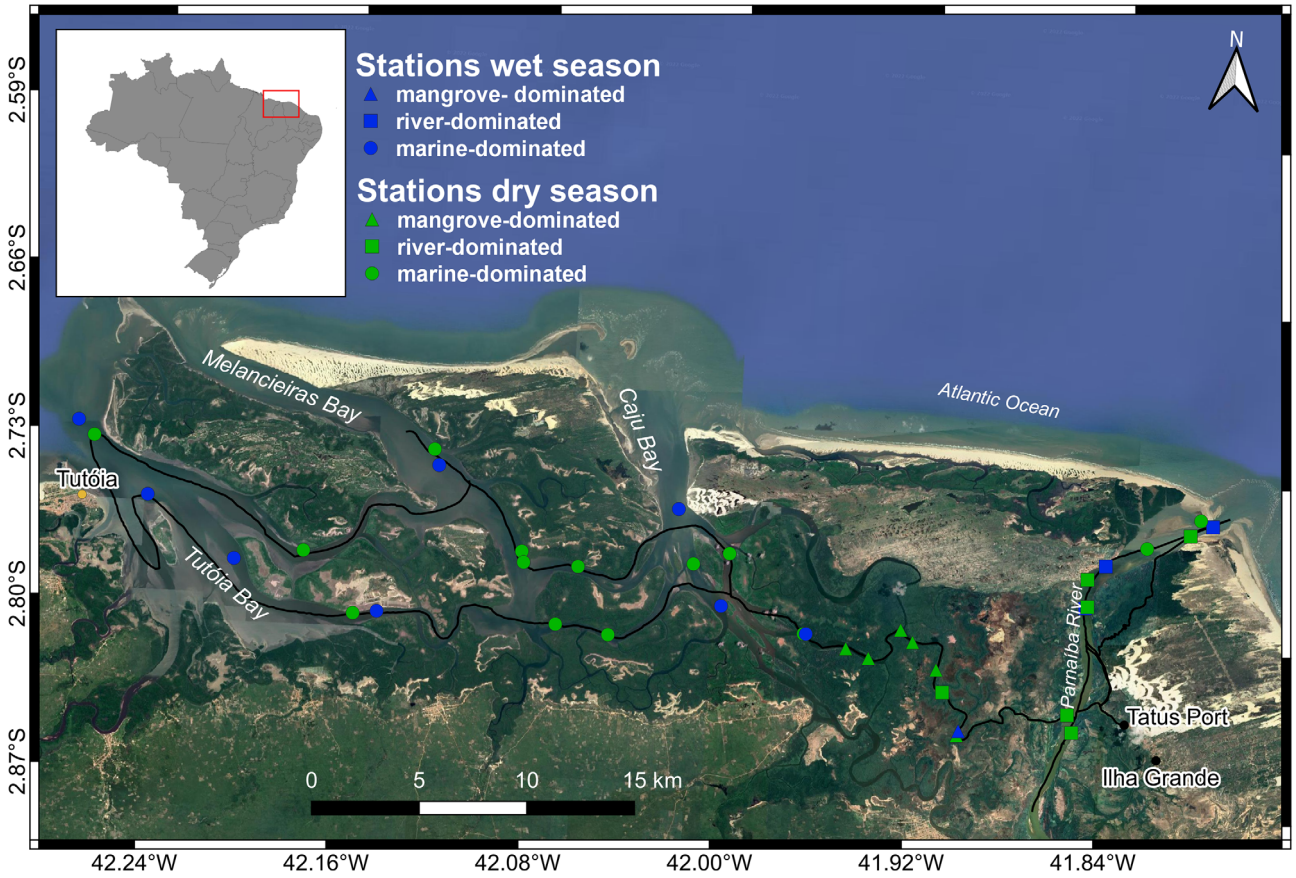

Fig. 1. Map of the sampled area, highlighting the discrete sampling points as grouped by the clusters (triangle: mangrove-dominated; square: river-dominated; and circle: marine-dominated), and the vessel trajectory (black line) along four channels of the Parnaíba delta: Parnaíba River, Caju, Melancieiras, and Tutóia bays. Samples were carried out in wet (blue) and dry (green) seasons.

sealed the bottles, stored them at a low temperature, and protected them from the light. TA was measured according to the methodology described by Dickson et al. (2007), using an automated open-cell potentiometric titration system. The precision of TA method was around 5 μmol.kg^{-1} ($n = 7$ measurements). TA values were adjusted according to certified reference material (CRM, A. G. Dickson from Scripps Institution of Oceanography). Samples for Chl *a* analysis were taken in 5 L polypropylene bottles. The water was filtered in Millipore® AP40 filters, and the filter was stored protected from the light, and frozen until analysis. The pigment was extracted from filters using 90% acetone, the extract was measured in a spectrophotometer, and pigment concentration was obtained according to Jeffrey and Humphrey (1975) equations.

CO_2 fluxes to the atmosphere

The net water-atmosphere CO_2 fluxes (F, mmol m^{-2} d^{-1}) were calculated using:

$$F = kK_0\left(pCO_2{}^{sw} - pCO_2{}^{atm}\right), \quad (3)$$

where K_0 is the solubility of CO_2 as a function of temperature and salinity (Weiss 1974), $pCO_2{}^{sw}$ is the pCO_2 in the estuarine waters and $pCO_2{}^{atm}$ is the atmospheric pCO_2 measured in situ, and k is the gas transfer velocity.

We used wind speed parametrizations specific for estuaries to determine the gas transfer velocity (Raymond and Cole 2001–RC; and Borges et al. 2004–BO). Furthermore, we also used a wind speed parameterization specific to open ocean waters (Wanninkhof 2014–WN) to provide ranges of estimations. The parametrizations are as follows:

$$k = 1.91^{*}\exp^{(0.35u)*}(600/\mathrm{Sc})^{-0.5}\,(\mathrm{RC}) \quad (4)$$

$$k = 4.045 + 2.58^{*}u^{0.758*}(600/\mathrm{Sc})^{-0.5}\,(\mathrm{BO}) \quad (5)$$

$$k = 0.251^{*}u^{2*}(600/\mathrm{Sc})^{-0.5}\,(\mathrm{WN}) \quad (6)$$

where Sc represents the Schmidt number, and u is the wind speed measured in situ.

Riverine CO_2 contribution to estuarine emissions

For the main river channel, we estimated the contribution of CO_2 originated within the estuarine zone and from the river to evaluate the relative contribution of riverine water in the estuarine CO_2 fluxes according to the method described in Rosentreter et al. (2018*b*). The relative contribution of the riverine CO_2 to the overall emissions in the estuary was calculated as:

$$\text{Riverine contribution}\,(\%) = \left(F_{\mathrm{River}}/F_{\mathrm{Estuary}}\right)^{*}100, \quad (7)$$

where F_{Estuary} is the average flux to the atmosphere in the main river channel (calculated from Eq. 3); and F_{River} is the riverine CO_2 flux to the estuary calculated from the estimated river discharge and riverine excess CO_2 (in mmol d^{-1}; Borges et al. 2006). The riverine excess CO_2 was calculated according to Abril et al. (2000):

$$\text{Riverine}\,CO_2\,\text{excess} = \mathrm{DIC}_{\text{in situ}} - \mathrm{DIC}_{\text{equilibrium}} \quad (8)$$

where $\mathrm{DIC}_{in\ situ}$ is the DIC at the river endmember and $\mathrm{DIC}_{\text{equilibrium}}$ represents the DIC calculated from the observed TA and pCO_2 values assuming equilibrium between the water and atmosphere CO_2 concentrations.

The DIC was estimated from pCO_2, TA, water temperature, and salinity using the CO2SYS program (Lewis and Wallace 1998). The dissociation constants for carbonic acid used were proposed by Mehrbach et al. (1973) refitted by Dickson and Millero (1987), and the borate acidity constant was obtained from Lee et al. (2010). We calculated the error propagation of DIC calculation following Orr et al. (2018). The combined uncertainty of DIC calculation was estimated to be ± 5 μmol kg^{-1}.

Conservative mixing lines

The conservative mixing of TA ($\mathrm{TA}_{\mathrm{mixing}}$) and DIC ($\mathrm{DIC}_{\mathrm{mixing}}$) were estimated according to Jiang et al. (2008), considering the inputs of the river significant:

$$C_{\mathrm{mixing}} = \frac{S_i}{S_{\mathrm{ocean}}} * C_{\mathrm{ocean}} + \left(1 - \frac{S_i}{S_{\mathrm{ocean}}}\right) * C_{\mathrm{river}}, \quad (9)$$

where S_i is the salinity in the sampling station, S_{ocean} is the salinity in the ocean endmember; the C_{ocean} is the variable concentration in the ocean endmember, and C_{river} the concentration in the riverine endmember.

The CO_2 mixing curve was estimated according to the $\mathrm{DIC}_{\mathrm{mixing}}$ and $\mathrm{TA}_{\mathrm{mixing}}$ values calculated from Eq. 9 through the CO2SYS program (Lewis and Wallace 1998), using the corresponding average temperature for the wet and dry seasons, and the constants stated before.

Categorization

Due to the great spatial and temporal heterogeneity of processes and locations in the PRD, a clustering analysis was performed to establish groups of similar stations for each season (dry and wet). A k-means cluster analysis was made based on the minimum Euclidean distances between the groups, using a standardized dataset of temperature, salinity, and pCO_2. The data were, then, grouped into the following clusters based on the k-means grouping and their characteristics: marine-dominated; river-dominated, and mangrove-dominated regions (Supporting Information Fig. S2).

Statistical analysis

Data normality was verified by the Shapiro–Wilk test. As most of the data did not present normal distribution,

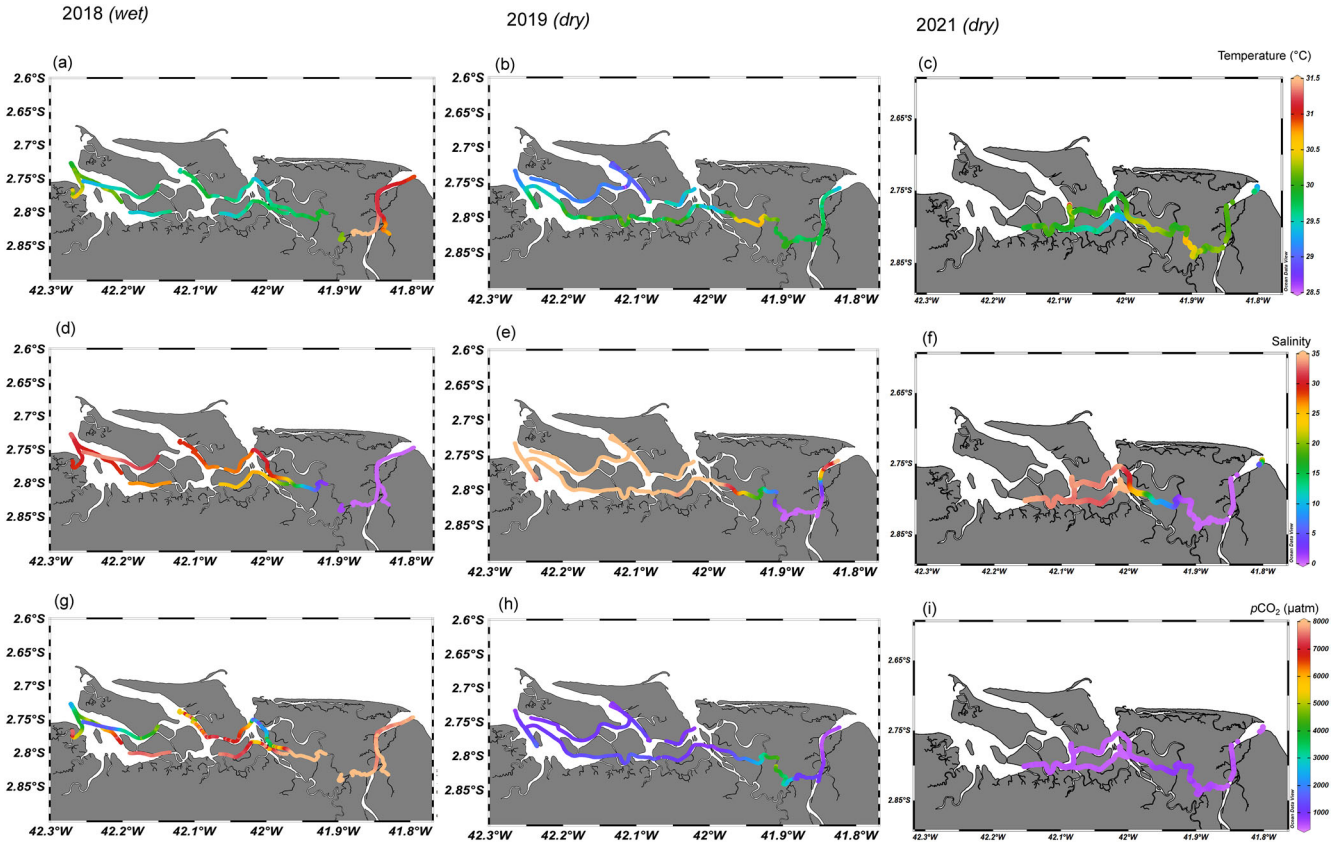

Fig. 2. Maps of the continuous measurements: temperature (**a–c**), salinity (**d–f**), and pCO_2 (**g–i**) spatial distribution in the PRD for each sampling campaign (2018: rainy season; 2019 and 2021: dry season).

non-parametric statistics were used. Spearman's rank correlation coefficient was used to investigate the correlation between variables, Wilcox to evaluate seasonal changes, and the difference between clusters was assessed by the Kruskal–Wallis test. A principal component analysis (PCA) was made with each seasonal dataset separately to identify patterns and processes in it. All statistical analyses were based on $\alpha = 0.05$ and were performed in R. Plots were created in Excel and R, and maps in Ocean Data View.

Results

Hydrological and biogeochemical conditions

Accumulated rainfall 1 week before sampling during the wet season was 47.4 mm in 2018. During the dry season, the accumulated rainfall reduced to 0.19 mm in 2019, and 2.0 mm in 2021. Following the seasonal pattern of the precipitation, the mean river discharge during the rainy season was 1345 $m^3\ s^{-1}$, while in the dry season it was 405 $m^3\ s^{-1}$ in 2019, and 577 $m^3\ s^{-1}$ in 2021. Overall, rainfall rates during sampling campaigns were lower than the historical average, while river discharge rates in 2018 and 2021 were higher than the historical average for the month sampled.

The main measured and calculated parameters in this study are summarized in Table S1 (Supporting Information). The river, mangrove and marine dominated regions were classified according to the cluster analysis (Supporting Information Fig. S2).

The spatial distribution of the continuous measurements is displayed in Fig. 2. During the field campaigns, the water temperature remained high and with little variation. However, the average water temperature in the dry season (29.78 ± 0.46°C) was significantly lower (p-value < 0.05) than in the rainy (30.12 ± 0.66°C). In addition, the marine-dominated areas presented the lowest temperatures in both seasons (dry = 29.62 ± 0.43°C; wet = 29.75 ± 0.29°C).

Salinity along the delta showed clear spatial and seasonal variability. During the rainy season, the delta was dominated by freshwater with an average salinity of 19.26 ± 13.18. The higher salinities during the rainy period were found particularly along the bays and near the river mouth, mainly during high tide. Salinities higher than 33 were found only during the dry season, when salinity was significantly higher (p-value < 0.05), with an average of 23.81 ± 15.43. In the dry season, the low salinity values were restricted to the river-dominated and mangrove-dominated regions, as shown in Fig. 2.

The carbonate system parameters (pH, TA, and DIC) also presented distinct spatial variability along the study area, with a significant positive relationship with salinity (Fig. 3). TA and DIC were always higher in the marine-dominated regions. In addition, strong seasonality was observed, with higher values found in the dry season compared to the wet season (Supporting Information Table S1). TA and DIC in the freshwater endmember showed a seasonal difference, with values of 412.0 and 464.6 μmol kg^{-1} in the rainy period, and 295.3 and 305.8 μmol kg^{-1} in the dry season, respectively.

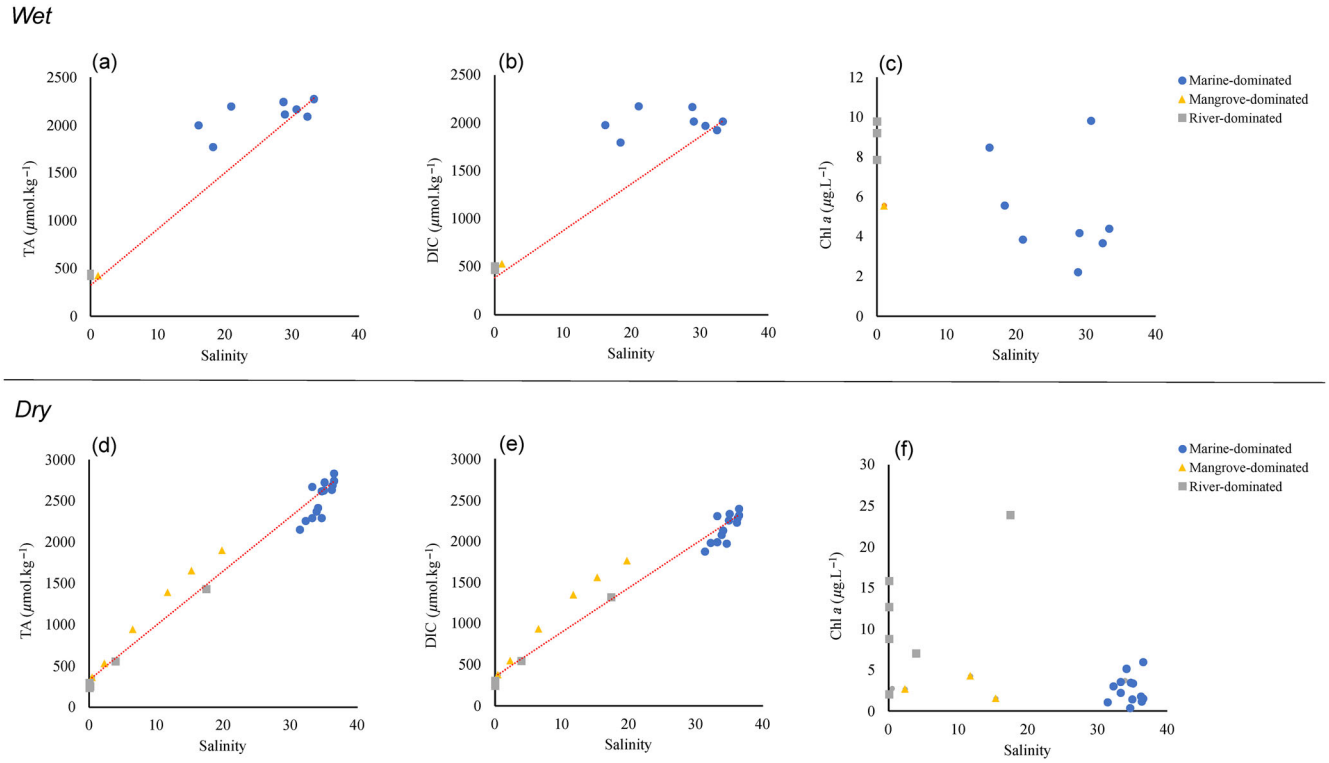

Fig. 3. Distributions of TA, DIC, and Chl *a* along the salinity gradient, for the wet (**a**–**c**), and dry (**d**–**f**) seasons. Red lines in (a, b, d) and (e) represent the two-endmember conservative mixing lines. The gray squares represent river-dominated regions, the yellow triangles are the mangrove-dominated regions, and the blue dots the marine-dominated areas.

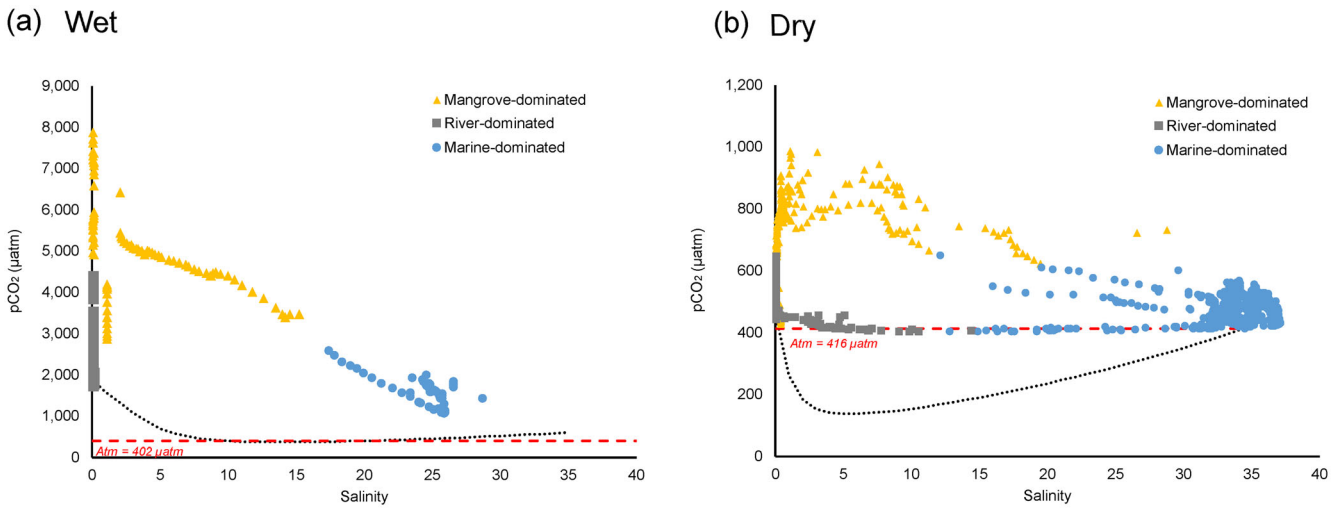

Fig. 4. Distribution of pCO_2 along the salinity gradient for the wet (**a**) and dry (**b**) seasons. Black dotted line indicates the conservative mixing, red dashed line is the atmospheric value. Colored by the clusters. Notice the different y scales.

In the rainy season, the deviation from the conservative mixing line for this season can be noticed more clearly in the marine-dominated areas. In contrast, during the dry season, TA and DIC distribution against salinity were nearer the conservative mixing line, with deviations found mostly in the mangrove-dominated regions, as observed in Fig. 3.

Overall, the delta was undersaturated in oxygen with respect to the atmosphere, but usually above 50%, however some few points exhibited values close to hypoxia. In both seasons, Chl *a* values dropped with a salinity increase, and, thus, Chl *a* values were lower during the dry season ($4.96 \pm 5.37\ \mu g\ L^{-1}$), mainly in the marine and mangrove-dominated waters. The river-dominated region was, in both seasons, the area with maximum Chl *a* levels (dry: $11.71 \pm 6.95\ \mu g\ L^{-1}$; wet: $8.97 \pm 0.82\ \mu g\ L^{-1}$).

pCO_2 and water-atmosphere CO_2 fluxes variability

Large spatial and seasonal variation in surface pCO_2 was observed within the deltaic system (p-value < 0.05), with values ranging from 406 to 7895 μatm (Fig. 2). In both seasons, surface pCO_2 was much higher in mangrove-dominated areas (dry: $736 \pm 107\ \mu$atm; wet: $5157 \pm 1256\ \mu$atm) than the other sampled areas. The lowest pCO_2 average was found in the marine-dominated regions (Supporting Information Table S1). In general, high values were associated with freshwater zones, and decreased with salinity. Indeed, in both seasons pCO_2 was significantly and negative correlated with salinity, and was, on average, almost four times higher during the wet season ($2006 \pm 1563\ \mu$atm) compared to the dry season ($527 \pm 113\ \mu$atm). The majority of pCO_2 values remained above the conservative mixing line (Fig. 4).

Due to no consensus of the best k-wind speed parametrization, in this study we used three different parameterizations, two of which are suitable for estuarine systems and one for open ocean waters. The use of three parametrizations gave us a large range of estimates. For this study, we used the average of these values. Overall, wind speed ranged from 0.32 to 14.98 m s^{-1} during the wet period, with direction predominantly from N and NE. Winds were slightly weaker during the dry period (4.28 ± 2.40 m s^{-1}) compared to the wet period (5.79 ± 2.51 m s^{-1}). There was significant spatial variability in the wind speed (p-value < 0.05). The mangrove-dominated regions presented the lowest mean wind velocity in both periods (dry = 3.03 ± 1.43 m s^{-1}; wet = 4.06 ± 2.23 m s^{-1}), compared to the marine-dominated regions (dry = 4.36 ± 2.39 m s^{-1}; wet = 5.96 ± 2.11 m s^{-1}), and the river-dominated area (dry = 5.46 ± 2.71 m s^{-1}; wet = 6.53 ± 3.28 m s^{-1}). The gas transfer velocity ranged from 0.69 to 245.25 cm.h^{-1} over the sampling campaigns. Following the seasonal changes observed in the wind speed, the gas transfer velocities were lower during the dry season (11.58 ± 12.32 cm h^{-1}) compared to the wet season (17.41 ± 15.90 cm h^{-1}). During both seasons, the highest values were found along the river dominated regions, and the lowest in the mangrove-dominated areas (Table 1).

The average flux of CO_2 using the three models ranged from 2 to 1494 mmol C m^{-2} d^{-1} in the rainy season, and from −2 to 119 mmol C m^{-2} d^{-1} in the dry season. The great majority of values were positive, indicating that the delta was mostly oversaturated in CO_2 in relation to the atmosphere (pCO_{2atm} average = 410 μatm), and the systems is an overall source of CO_2 to the atmosphere. The negative values were restricted to the areas with high salinity. The large spatial variability found in pCO_2 values and wind speed was reflected in the fluxes, resulting in a high standard deviation (Supporting Information Fig. S3). There was significant seasonal and spatial variability for the fluxes (p-value < 0.005). Averaged fluxes were approximately 20 times lower in the dry season (9 ± 11 mol m^{-2} d^{-1}) than during the rainy season (210 ± 251 mmol m^{-2} d^{-1}). The mangrove-dominated areas were a stronger source of CO_2 in the rainy season (434 ± 290 mmol m^{-2} d^{-1}) and a moderate source during the dry season (22 ± 13 mmol m^{-2} d^{-1}). In contrast, the marine-dominated regions had the lowest values of fluxes in the wet season (100 ± 90 mmol m^{-2} d^{-1}) and in the dry season (5 ± 7 mmol m^{-2} d^{-1}). The river-dominated region was a stronger source of CO_2 during the rainy season (410 ± 336 mmol m^{-2} d^{-1}) when compared to the dry season (11 ± 11 mmol m^{-2} d^{-1}).

Discussion

Spatial–temporal variability of TA and DIC

Salinity plays an important role in the spatial and seasonal variability of the carbonate system in the PRD. During the rainy period, when river discharge is high, the salinity gradient extended toward the platform. The oceanic waters adjacent to the delta present typical values of salinity close to 36 (da Silva et al. 2015; Carvalho et al. 2017), but our maximal measured salinity in the wet period was 33.5. The fraction of freshwater, estimated following Bianchi (2007), was 99% at the river-dominated waters, 90% at the mangrove-dominated and 21% at the marine-dominated regions during the wet season. This is a general estimate, using the salinity average values, and can be subject to errors, as there are other factors involved, such as the tide variability. A better evaluation of the freshwater contribution in the PRD is an important topic to be assessed in future studies. Nevertheless, our estimate suggests that, currently, the estuarine region occupies an extensive area of the Delta. The freshwater input can come from the connecting channel, surface runoff or from small rivers that drain into this system (da Silva et al. 2015; Smith et al. 2021).

In opposition, during the dry period, with reduced river flow and runoff, high salinity waters are spread in all the compartments of the PRD (Fig. 2). The freshwater fraction was reduced, especially at the marine-dominated regions (5%), but it was still high at the river-dominated waters (97%), and at the mangrove-dominated ones (93%). The salinity gradient was found approaching the mouth of the main channel and in the secondary channel connecting the delta to the coastal embayment. There is a relationship between rainfall and the

Table 1. Average (± standard deviation), minimum and maximum values of the calculated fluxes in the PRD, according to the parametrization used, divided by season, and grouping. WN14 refers to parametrization described in (Wanninkhof 2014); RC01 to (Raymond and Cole 2001); and BO04 to (Borges et al. 2004).

			Wind speed	Flux (BO04)	Flux (RC01)	Flux (WN14)	*k* (WN14)	*k* (RC01)	*k* (BO04)	Flux	*k*
			$m\ s^{-1}$	$Mmol\ m^{-2}\ d^{-1}$	$Mmol\ m^{-2}\ d^{-1}$	$Mmol\ m^{-2}\ d^{-1}$	$cm\ h^{-1}$	$cm\ h^{-1}$	$cm\ h^{-1}$	$Mmol\ m^{-2}\ d^{-1}$	$cm.h^{-1}$
Wet	Mangrove-dominated	Average	4.06	622	462	218	5.4	11.3	14.4	434	10.4
		SD	2.23	267	440	211	5.7	12.3	6.2	290	7.8
		Min	0.32	66	64	1	0.0	2.1	2.2	44	1.5
		Max	10.33	1224	2386	900	26.8	71.1	30.2	1433	42.7
	River-dominated	Average	6.53	385	610	235	13.4	36.3	20.8	410	23.5
		SD	3.28	193	676	201	11.9	44.9	8.2	336	21.2
		Min	1.04	98	48	5	0.3	2.7	5.3	51	2.8
		Max	13.10	1017	2618	926	43.1	187.5	36.1	1494	88.9
	Marine-dominated	Average	5.96	119	122	59	10.0	21.8	19.6	100	17.2
		SD	2.11	78	172	49	7.2	33.2	5.5	90	14.6
		Min	0.44	5	3	0	0.0	2.2	2.7	2	1.7
		Max	14.98	388	2086	372	56.3	361.0	40.0	881	152.4
Dry	Mangrove-dominated	Average	3.03	36	20	9	2.8	6.4	11.7	22	6.9
		SD	1.43	18	15	9	2.7	4.1	4.2	13	3.6
		Min	0.33	2	1	0	0.0	2.1	2.2	1	1.5
		Max	8.36	105	146	72	17.5	35.6	25.7	108	26.3
	River-dominated	Average	5.46	13	13	6	9.3	20.1	18.1	11	15.9
		SD	2.71	11	17	7	7.9	20.7	7.2	11	11.6
		Min	0.48	−1	−1	−1	0.1	2.3	2.9	−1	1.8
		Max	12.28	57	165	55	37.9	140.5	34.4	92	70.9
	Marine-dominated	Average	4.36	7	6	3	6.2	14.2	15.3	5	11.9
		SD	2.39	6	14	4	7.0	29.8	6.4	7	13.5
		Min	0.01	−2	−2	−1	0.0	1.9	0.2	−2	0.7
		Max	16.54	40	302	33	68.7	624.0	43.1	119	245.3

river discharge, but it was observed in other studies that the discharge does not reach values bellow 261 $m^3 s^{-1}$ in the dry season, probably due to its regulation by the Boa Esperança reservoir upstream (da Silva et al. 2015), and may explain the low salinities in the main river channel. Furthermore, the water from lateral diffusion coming from the huge mangrove forest (Supporting Information Fig. S4) and dunes can also contribute to the low salinity in the mangrove-dominated channel (Dias et al. 2016). This lateral diffusion refers to the water that leaves the mangrove forest during ebb tide, related to the hydrodynamics of the mangrove forest, the rainfall, and driven by the tidal variability and exchange with porewater, also known as tidal pumping (Ovalle et al. 1990; Stieglitz et al. 2013; Call et al. 2019).

The two endmembers mixing model is commonly used to examine if there is significant production or consumption of organic and inorganic carbon species along the land-ocean aquatic continuum throughout the deviation from the conservative mixing behavior. The significant correlations between DIC, TA and salinity in both seasons suggest a high influence of the mixing processes, as some sampled stations followed nearly the conservative lines (Fig. 3). However, certain stations presented deviation above the conservative trend, evidencing an addition of DIC and TA in the estuary, possibly reflecting the biogeochemical processes caused by the tidal pumping processes in the large mangrove forest area of the delta. The interstitial waters, which are enriched in DIC, TA, greenhouse gases, and other compounds as the result of aerobic and anaerobic organic matter degradation that occur in mangrove soils, are then transported from the mangrove creeks to estuarine and continental shelf waters (Bouillon et al. 2005; Maher et al. 2015; Sippo et al. 2016).

The deviations from conservative mixing lines of TA (ΔTA) as a function of DIC (ΔDIC) can tell us about the main diagenetic processes taking place during organic matter degradation in mangroves that contribute to alkalinity generation (Borges et al. 2003; Bouillon et al. 2005). The relationship between ΔTA and ΔDIC found in the PRD, indicates a combination of aerobic and anaerobic sulfate reduction and denitrification as the diagenetic pathways of the processes of organic matter degradation, producing TA and DIC (Fig. 5), which is consistent with other mangrove-dominated estuaries (Borges et al. 2003; Bouillon et al. 2007; Cotovicz et al. 2020*b*; Reithmaier et al. 2020; Santos et al. 2021). The low concentrations of total nitrogen (TN) in PDR, available only in the main river channel (0.47 ± 0.11 mg L^{-1}, Paula Filho et al. 2020), indicates that the denitrification is probably a minor pathway of TA production, as observed in other pristine mangrove creeks (Maher et al. 2015). It is suggested that the production of DIC and TA, and consequent outwelling of carbon by mangrove tidal creeks, with later ocean storage, may represent an important fraction of the blue carbon sequestration with a potential significance in global carbon budgets (Call et al. 2014; Santos et al. 2021). Indeed, ~50% of the carbon fixed by mangroves are not accounted for (Bouillon et al. 2008), but recent studies hypothesized that the outwelling of DIC can explain a major part of this "missing mangrove carbon" (Maher et al. 2018; Santos et al. 2021).

Some stations, mainly in the dry season, presented deviation below the conservative mixing (negative values; Fig. 3). This suggests that process of reoxidation might be occurring in certain regions of the delta, i.e., the TA and DIC are being consumed due to sulfide reoxidation (Cotovicz et al. 2021). Sulfate reduction is a process which generates TA, however most of the sulfide produced is reoxidized, resulting in an alkalinity consumption (Middelburg et al. 2020). A net gain of TA occurs only if the sulfate reduction is coupled to processes that consume permanently the reduced compounds, like the pyrite formation (Middelburg et al. 2020; Reithmaier et al. 2020). Indeed, pyrite stocks were correlated to TA export in mangrove tidal creeks (Reithmaier et al. 2020). In Fig. 3, it is possible to see that these negative values are restricted to high salinity areas, which are more oxygenated (Supporting Information Table S1). Therefore, not all DIC and TA produced in the mangroves of the delta are being exported, as a part seems to be reoxidized.

Drivers of pCO_2 variability

The pCO_2 distribution along the salinity gradient displayed in Fig. 4 represents the distinct spatial and seasonal variations in the PRD, suggesting that there are multiple factors influencing the carbon dynamics. The pCO_2 measurements were well above the conservative mixing curve, particularly in the low salinity zones of the river-dominated region, and in the mangrove-dominated areas. In the river-dominated waters, the excess of CO_2 can be attributed to the riverine-CO_2 that enters the estuary, especially during the high discharge season. In fact, the contribution of riverine CO_2 to the overall CO_2 emission in the main channel was estimated to be around 75% in the rainy season. Freshwater runoff from rivers is an important source of CO_2 in estuaries and can contribute on average to 10% of total estuarine emissions (Abril and Borges 2005), or more (Rosentreter et al. 2018*b*). The freshwater influence was also observed in other tropical deltas, such as the Mekong and Guayas, which presented higher values of pCO_2 in the inner areas of the estuary during the high discharge season (Borges et al. 2018; Belliard et al. 2022).

In contrast, in the dry season, the pCO_2 in the river-dominated waters was much lower, and the contribution of riverine-CO_2 was around 45% of the total CO_2 estuarine emissions. This reduction could be associated with enhanced phytoplankton primary production, as the Chl *a* values were higher in the dry season in this area (11.71 ± 6.95 μg/L). In the Mekong Delta, the authors associated the decrease in the pCO_2 values of the inner estuary with a reduction of the residence time in the low water season, which favored the growth of freshwater phytoplankton (Borges et al. 2018). Furthermore, the more saline conditions during dry season explained the

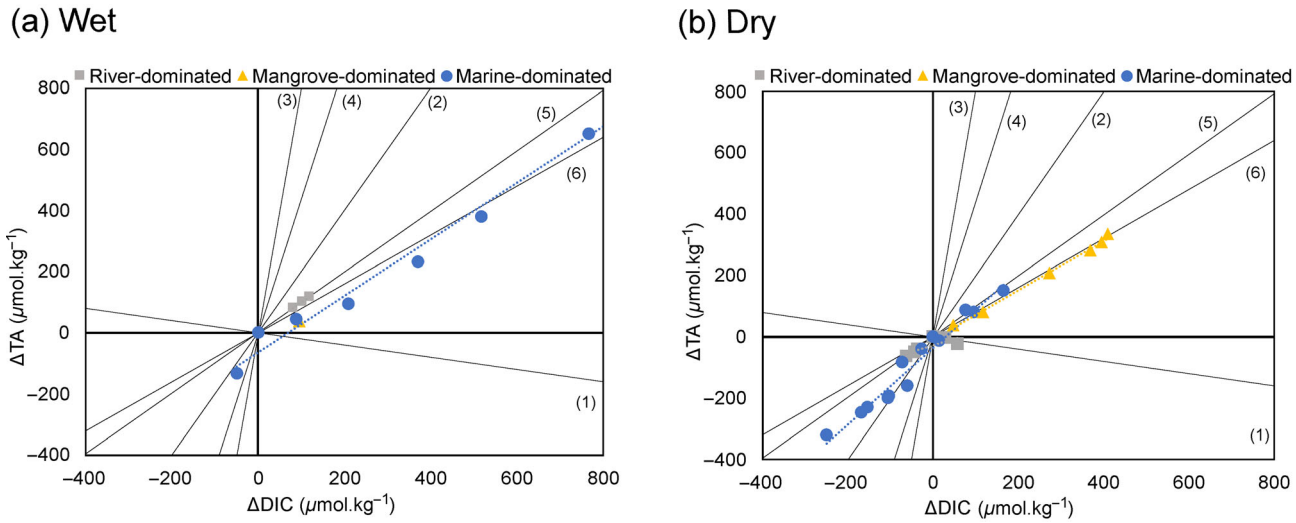

Fig. 5. ΔTA vs. ΔDIC for the (**a**) wet and (**b**) dry season. Dotted black lines indicate the stoichiometry of the main processes that influence alkalinity and DIC: (1) aerobic respiration, (2) carbonate dissolution, (3) iron reduction, (4) manganese reduction, (5) sulfate reduction, and (6) denitrification, which were calculated according to Middelburg et al. (2020).

low values in the delta. Previous study showed that adjacent shelf waters present typical values of pCO_2 around 400 μatm (Carvalho et al. 2017). Moreover, undersaturated conditions relative to atmospheric equilibrium were observed only at the main river mouth and in a portion of marine-dominated waters (Fig. 4) during the dry season. This could be caused by the more intense marine intrusion, the thermodynamic equilibration during the mixing of fresh and seawater, and by the biological uptake (Cotovicz et al. 2020*a*; Abril et al. 2021).

Although mangroves are an important blue carbon environment, mangrove dominated waters usually have CO_2 concentrations highly above than the estuary associated (Borges et al. 2003). In the PRD, the mean pCO_2 values observed in the mangrove-dominated waters are within the range reported in other mangrove systems in the world (Bouillon et al. 2007; Akhand et al. 2016; Rosentreter et al. 2018*a*; Call et al. 2019; Cotovicz et al. 2020*a*; Belliard et al. 2022). Maximum pCO_2 values were found along these areas, fairly exceeding the values calculated by the mixing curve, in both seasons (Fig. 4). The presence of processes that add CO_2 in the system through the mangrove tidal pumping (Jeffrey et al. 2018; Call et al. 2019), the intense mineralization of organic matter from autochthonous and allochthonous sources (Borges et al. 2018) and the heterotrophic processes related to the high availability of mangrove-derived organic matter, during the rainy season, could sustain these elevated levels of $pCO2$ (Borges and Abril 2010).

In opposition, during the dry season, the significant reduction of the pCO_2 levels in the mangrove-dominated areas can be related foremostly to the intrusion of seawater. The PRD is a distinct delta that has gone through a lob switching process (Smith et al. 2021). Its western part, where we find the large bays and multiple mangrove creeks, is almost independent of the river (da Silva et al. 2015), and its format can favor the seawater intrusion, significantly reducing the pCO_2 values (Borges et al. 2018). This reduction is also observed in other mangrove-dominated systems, such as the large Sundarbans, where there is a predominance of the waters from the Bay of Bengal, with low pCO_2 and high buffering capacity (Akhand et al. 2021*a*). The TA : DIC ratio in the PRD, used to give information regarding the buffering capacity of seawater was, on average, close to or below 1 in river and in mangrove-dominated waters indicating a low buffering capacity in these regions associated with low pH (Egleston et al. 2010). Overall, rivers deliver more acidified waters (low TA : DIC and pH) to estuaries (Borges and Abril 2010; Cai et al. 2021). By contrast, in marine-dominated regions, the TA/DIC and pH values increase as the result of the intrusion of well-buffered seawater in the estuary, particularly in the bays (Supporting Information Fig. S3).

There was a weak correlation of pCO_2 and DO% during the dry season ($r^2 = -0.55$, $p < 0.05$), and a no significant correlation during the rainy season (Supporting Information Fig. S4). This kind of pattern can occur in some estuaries in regions dominated by mangrove influence (Akhand et al. 2016; Cotovicz et al. 2020*a*), distinguishing from other ecosystems, where the regulation of pCO_2 levels is primarily controlled by planktonic organic matter production and respiration (Cotovicz Jr et al. 2015). This suggests that, although the aerobic organic matter respiration in the PRD is an important source of CO_2, the excess CO_2 is also likely related to the anaerobic bacterial metabolism in water and sediments (Hamilton et al. 1995), such as the sulfate reduction and denitrification, in mangrove tidal creeks (Borges and Abril 2010).

The Chl *a* values in the PRD indicate the importance of primary productivity. The higher values observed along the main

channel, particularly during the dry season, may be supported by the availability of nutrients, as seen in another part of the PRD (dos Santos Costa and Cutrim 2021). However, despite some high values of Chl *a* observed in the PRD, the values of pCO_2 remained largely oversaturated and no correlation was observed between Chl *a* and pCO_2. This confirms that the production and export of CO_2 by the heterotrophic metabolism is much stronger than the autotrophic CO_2 uptake. The marine and mangrove-dominated regions had lower Chl *a* values, particularly during the dry season, as these areas were strongly influenced by the intrusion of oligotrophic seawater with low Chl *a* values.

The PRD is a unique environment composed by distinct ecosystems. In both seasons, the areas sampled were statistically different regarding the parameters that constitute the carbon cycle. These differences indicated that the pCO_2 variability and fluxes are controlled by combining factors, as shown in the PCA in Fig. 6. In both seasons, the PCA returned two PCs that account for more than 70% of the data variance. The loadings from the PCA clearly illustrate the processes and spatial distribution of the stations. The river-dominated waters presented more influence by Chl *a* and temperature, but as freshwaters exhibited lower TA and DIC. This result is consistent with previous studies of tropical river estuaries in Brazil, which have found that the river endmember tends to be poorly buffered (Cotovicz et al. 2020*b*). In the mangrove-dominated regions, the high pCO_2 showed the importance of the lateral residual fluxes, which increase the TA, DIC, and pCO_2 via the exchange with porewater (Maher et al. 2015), and are strongly dependent on the huge mangrove forest area (Alongi and Brinkman 2011). In the marine-dominated areas, an increase in DO%, TA and DIC was observed as pCO_2 decreased, representing a seawater domain with high buffering capacity. During the dry season, all parameters were influenced and diluted by the intense seawater intrusion.

The CO_2 emissions in a global context

Estuarine systems and mangrove-dominated waters are, mainly, sources of CO_2 to the atmosphere, and significant in regional and global carbon budgets (Chen et al. 2013; Laruelle et al. 2013). However, the deltaic estuarine system of the Parnaíba river presents a huge spatial, ecological, and biogeochemical complexity compared to typical estuaries. Therefore, generalizations must be considered with caution. The supersaturated levels of CO_2 in surface water with respect to the atmospheric levels showed the PRD as a strong annual source of CO_2. The average flux in the rainy season (210 ± 251 mmol m^{-2} d^{-1}) is one of the largest fluxes found in estuaries around the world (Chen et al. 2013) and was highly above (four-fold higher) the global average CO_2 emissions from mangrove-dominated estuaries in the region between 0 and 23.5°S (52.1 ± 16.1 mmol m^{-2} d^{-1}; Rosentreter et al. 2018*a*), and also three-fold higher than the most recent global estimate at 75.4 mmol m^{-2} y^{-1} (Call et al. 2019). However, the average CO_2 flux in the dry season (9 ± 11 mmol m^{-2} d^{-1}) is 20 times lower than the average of the rainy season.

The regions dominated by mangroves exhibited the highest fluxes, as expected in mangrove-dominated channels in relation to the associated estuary (Borges et al. 2003). The estimated mangrove area in the delta is ~1500 km^2, accounting for roughly 1% of the global mangrove forest area (Giri et al. 2011). Based on this area and the fluxes in the mangrove channels, we can extrapolate that the PRD emits ~0.34 Tg C yr^{-1} annually, which corresponds to 1% of the global emissions from mangrove systems (34.3 Tg C yr^{-1}; Rosentreter et al. 2018*a*). During the rainy season, this contribution increases to about 2.7%, as the emissions from the mangrove area in the delta reach 0.94 Tg C yr^{-1}. These estimates were obtained using seasonal weighted averages, considering ~121 rainy days per year and 244 dry days per year (Supporting

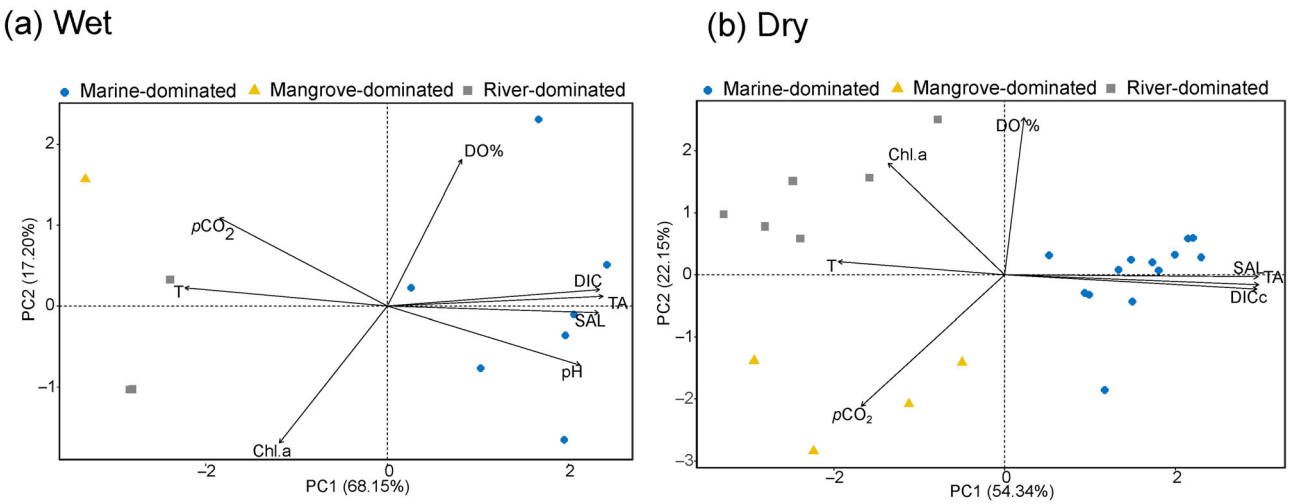

Fig. 6. PCA for rainy (**a**) and dry (**b**) seasons based on the discrete sampled stations, divided in high salinity areas (blue dots), mangrove-dominated (yellow triangles) and river-dominated waters (gray squares).

Information Fig. S1). However, it is important to note that this annual estimate may overestimate or underestimate the fluxes, as this study did not consider different tide regimes or transitional seasons. In addition, the CO_2 emissions from mangrove soil are not included in our estimate. Still, since CO_2 fluxes from these sediments are similar to fluxes from mangrove waters (Bouillon et al. 2008), this would not significantly influence our estimate.

The marked seasonal variability of fluxes found in the PRD was also found in other estuarine systems (Jiang et al. 2008; Sarma et al. 2012; Akhand et al. 2016; Rosentreter et al. 2018*a*, 2018*b*; Cotovicz et al. 2020*a*; Akhand et al. 2021*a*, 2021*b*), and it is mostly related to the seasonality of the saline intrusion and the freshwater discharge. Riverine-CO_2 may contribute largely to estuarine CO_2, mainly in those estuaries associated with large discharge rates and low residence times (Joesoef et al. 2015; Rosentreter et al. 2018*b*). River-dominated estuaries are usually stronger sources of CO_2 due to the entrance of this allochthonous river CO_2 (Jiang et al. 2008), as it was observed in the main channel of the river and two creeks of PRD by Chielle et al. (2023). But the seasonal augment of the marine intrusion and the reduced river water supply can significantly change the carbon dynamics and the CO_2 efflux along the delta. Seawater with high carbonated buffering capacity could restrain the effect of pCO_2 generated in the mangroves and lower the CO_2 emission (Akhand et al. 2021*a*, 2021*b*).

Projections point to the intensification of droughts, rising sea levels, and warming as a consequence of climate change on the northeastern coast of Brazil (Soares et al. 2021), which are likely to increase the salinization of groundwater, surface water, and soils (IPCC et al. 2019). The increase in aridity worldwide together with anthropogenic pressure will negatively impact ecosystems, altering their carbon dynamics (Bauer et al. 2013; Regnier et al. 2013). Only few studies accesses the carbon dynamics in arid and semi-arid environments (Leopold et al. 2017; Yao and Hu 2017; Marins et al. 2023), but they mostly lack a seasonal focus. In these systems, heating and evaporation have a strong additional influence on water chemistry and dynamics (Dias et al. 2016; Cavalcante et al. 2021). Studies have shown that the decreasing freshwater inputs from rivers are related to low CO_2 emissions in estuarine and mangrove-dominated waters. This is attributed to the low inputs of DIC (and CO_2) from river sources, as well as the limited lateral exchanges between mangroves and estuarine waters during periods of low river flow (Sarma et al. 2011, 2012; Cotovicz et al. 2020*a*; Akhand et al. 2021*a*, 2021*b*; Belliard et al. 2022). Therefore, the significant reduction of CO_2 emissions in the PRD with the entrance of seawater may represent a prognostic of what would happen in some estuarine systems in a climate change scenario.

The PRD is a key environment in evaluating this kind of change since it is a mostly preserved environment inserted in an EPA, where the variability of natural factors, such as river discharge and rainfall, are the main drivers of shoreline changes (Ferreira et al. 2021). A trend of reduction in the number of rainy days and precipitation in the coastal region of NE Brazil (de Carvalho et al. 2020) together with a shoreline retreat in the western part of the PRD (Ferreira et al. 2021) can result in stronger seawater intrusion and significantly impact the carbon dynamic in the delta, and potentially in other estuarine systems.

Conclusions

The PRD is the largest open sea delta in the Americas, a heterogeneous complex system with extensive mangrove forests, a variety of channels, large bays and with a very extensive estuarine area. Our data shows that the delta is a source of CO_2 to the atmosphere with well-marked spatial and seasonal variability. Primary productivity, mineralization of organic matter, river-ocean mixing, and carbonate thermodynamic equilibrium are the main processes driving the pCO_2 variability in this system. The huge mangrove forest area contributes with residual lateral fluxes and excess of TA and DIC to estuarine waters. The seasonality in the pCO_2 values and CO_2 emissions indicate a strong control by the marine intrusion and the river discharge. The high seawater intrusion in most channels of the delta promoted a significant decrease in the pCO_2 values and increased the buffering capacity, reducing the CO_2 degassing about 20-fold compared to the wet season. This may highlight an important prognostic of sea level rise and the reduction of precipitation and freshwater discharge in this type of mangrove-dominated system. Therefore, the outlook of aquatic CO_2 emissions in the delta depends mainly on the levels of freshwater discharge, the seawater intrusion in the delta, and the maintenance of the mangrove forest. The large variability between and within estuarine systems, and the strong seasonal changes, highlight the importance of improving our understanding of estuarine air-water CO_2 fluxes, especially in highly heterogeneous tropical estuaries.

Data availability statement

The data that support the findings of this study are available by contacting the corresponding author, who will make sure data is available under reasonable request.

References

Abril, G., H. Etcheber, A. V. Borges, and M. Frankignoulle. 2000. Excess atmospheric carbon dioxide transported by rivers into the Scheldt estuary. C. R. Acad. Sci. **330**: 761–768.

Abril, G., B. G. Libardoni, N. Brandini, L. C. Cotovicz, P. R. P. Medeiros, G. H. Cavalcante, and B. A. Knoppers. 2021. Thermodynamic uptake of atmospheric CO2 in the oligotrophic and semiarid São Francisco estuary (NE Brazil). Mar. Chem. **233**: 103983. doi:10.1016/j.marchem.2021.103983

Abril, G., and A. V. Borges. 2005. Carbon dioxide and methane emissions from estuaries. *In* A. Tremblay, L. Varfalvy, C. Roehm, and M. Garneau [eds.], Greenhouse gas emissions—fluxes and processes, Environmental Science. Springer, Berlin, Heidelberg. doi:10.1007/978-3-540-26643-3_8

Akhand, A., and others. 2016. A comparison of CO2 dynamics and air-water fluxes in a river-dominated estuary and a mangrove-dominated marine estuary. Geophys. Res. Lett. **43**: 11726–11735. doi:10.1002/2016GL070716

Akhand, A., A. Chanda, K. Watanabe, S. Das, T. Tokoro, K. Chakraborty, S. Hazra, and T. Kuwae. 2021*a*. Low CO2 evasion rate from the mangrove-surrounding waters of the Sundarbans. Biogeochemistry **153**: 95–114. doi:10.1007/s10533-021-00769-9

Akhand, A., A. Chanda, K. Watanabe, S. Das, T. Tokoro, S. Hazra, and T. Kuwae. 2021*b*. Reduction in riverine freshwater supply changes inorganic and organic carbon dynamics and air-water CO2 fluxes in a tropical mangrove dominated estuary. J. Geophys. Res. Biogeosci. **126**: e2020JG006144. doi:10.1029/2020JG006144

Alongi, D. M., and R. Brinkman. 2011. Forest hydrology and biogeochemistry: synthesis of past research and future directions. Spinger, p. 203–219.

Alongi, D. M. 2012. Carbon sequestration in mangrove forests. Carbon Manag. **3**: 313–322. doi:10.4155/cmt.12.20

Bauer, J. E., W.-J. Cai, P. A. Raymond, T. S. Bianchi, C. S. Hopkinson, and P. A. G. Regnier. 2013. The changing carbon cycle of the coastal ocean. Nature **504**: 61–70.

Belliard, J.-P., and others. 2022. Carbon dynamics and CO2 and CH4 exchange in the mangrove dominated Guayas river delta, Ecuador. Estuar. Coast. Shelf Sci. **267**: 107766. doi:10.1016/j.ecss.2022.107766

Bianchi, T. S. 2007. Biogeochemistry of estuaries. Oxford Univerisity Press, p. 688.

Borges, A. V., S. Djenidi, G. Lacroix, J. Théate, B. Delille, and M. Frankignoulle. 2003. Atmospheric CO2 flux from mangrove surrounding waters. Geophys. Res. Lett. **30**: 1558. doi:10.1029/2003GL017143

Borges, A. V., J. P. Vanderborght, L. S. Schiettecatte, F. Gazeau, S. Ferrón-Smith, B. Delille, and M. Frankignoulle. 2004. Variability of the gas transfer velocity of CO_2 in a macrotidal estuary (the Scheldt). Estuaries **27**: 593–603. doi:10.1007/BF02907647

Borges, A. V., L. S. Schiettecatte, G. Abril, B. Delille, and F. Gazeau. 2006. Carbon dioxide in European coastal waters. Estuar. Coast. Shelf Sci. **70**: 375–387. doi:10.1016/j.ecss.2006.05.046

Borges, A. V., Abril, G. (2010). Carbon dioxide and methane dynamics in estuaries. In EGU General Assembly Conference Abstracts, p. 10812.

Borges, A. V., G. Abril, and S. Bouillon. 2018. Carbon dynamics and CO2 and CH4 outgassing in the Mekong delta. Biogeosciences **15**: 1093–1114.

Bouillon, S., F. Dehairs, A. V. Borges, and B. Velimirov. 2005. Biogeochemistry of the tana estuary and delta (northern Kenya). Glob. Biogeochem. Cycles **52**: 40. doi:10.1029/2004GB002267

Bouillon, S., F. Dehairs, B. Velimirov, G. Abril, and A. V. Borges. 2007. Dynamics of organic and inorganic carbon across contiguous mangrove and seagrass systems (Gazi Bay, Kenya). J. Geophys. Res. **112**: 2018. doi:10.1029/2006JG000325

Bouillon, S., and others. 2008. Mangrove production and carbon sinks: A revision of global budget estimates. Glob. Biogeochem. Cycles **22**: 1–12. doi:10.1029/2007GB003052

Cai, W. J. 2011. Estuarine and coastal ocean carbon paradox: CO2 sinks or sites of terrestrial carbon incineration? Annu. Rev. Mar. Sci. **3**: 123–145. doi:10.1146/annurev-marine-120709-142717

Cai, W.-J., and others. 2021. Natural and anthropogenic drivers of acidification in large estuaries. Annu. Rev. Mar. Sci. **13**: 1–33. doi:10.1146/annurev-marine-010419-011004

Call, M., and others. 2014. Spatial and temporal variability of carbon dioxide and methane fluxes over semi-diurnal and spring-neap-spring timescales in a mangrove creek. Geochim. Cosmochim. Acta **150**: 211–225. doi:10.1016/j.gca.2014.11.023

Call, M., I. R. Santos, T. Dittmar, C. E. de Rezende, N. E. Asp, and D. T. Maher. 2019. High pore-water derived CO2 and CH4 emissions from a macro-tidal mangrove creek in the Amazon region. Geochim. Cosmochim. Acta **247**: 106–120. doi:10.1016/J.GCA.2018.12.029

Carvalho, A. C. O., R. V. Marins, F. J. S. Dias, C. E. Rezende, N. Lefèvre, M. S. Cavalcante, and S. A. Eschrique. 2017. Air-sea CO2 fluxes for the Brazilian northeast continental shelf in a climatic transition region. J. Mar. Syst. **173**: 70–80. doi:10.1016/j.jmarsys.2017.02.013

Cavalcante, M. S., R. V. Marins, F. J. S. Dias, and C. E. Rezende. 2021. Assessment of carbon fluxes to coastal area during persistent drought conditions. Reg. Stud. Mar. Sci. **47**: 101934. doi:10.1016/j.rsma.2021.101934

Chen, C. T., T. H. Huang, Y. C. Chen, Y. Bai, X. He, and Y. Kang. 2013. Air-sea exchanges of CO2 in the world's coastal seas. Biogeosciences **10**: 6509–6544. doi:10.5194/bg-10-6509-2013

Chen, X., F. Zhang, Y. Lao, X. Wang, J. Du, and I. R. Santos. 2018. Submarine groundwater discharge-derived carbon fluxes in mangroves: An important component of blue carbon budgets? J. Geophys. Res. Oceans **123**: 6962–6979. doi:10.1029/2018JC014448

Chielle, R. S. A., R. V. Marins, F. J. S. Dias, K. K. Borges, and C. E. Rezende. 2023. Contributions from the main river of the largest open sea delta in the Americas to the CO2 fluxes. Reg. Stud. Mar. Sci. **62**: 102922. doi:10.1016/j.rsma.2023.102922

Cole, J. J., and others. 2007. Plumbing the global carbon cycle: Integrating inland waters into the terrestrial carbon budget. Ecosystems **10**: 172–185.

Cotovicz, L. C., Jr., B. A. Knoppers, N. Brandini, S. J. Costa Santos, and G. Abril. 2015. A large CO2 sink enhanced by eutrophication in a tropical coastal embayment (Guanabara Bay, Rio de Janeiro, Brazil). Biogeoscience **12**: 4671–4720.

Cotovicz, L. C., R. Chielle, and R. V. Marins. 2020*a*. Air-sea CO2 flux in an equatorial continental shelf dominated by coral reefs (southwestern Atlantic Ocean). Cont. Shelf Res. **104**: 175. doi:10.1016/j.csr.2020.104175

Cotovicz, L. C., and others. 2020*b*. Sources and sinks of CO2 in the delta of the Paraíba do Sul River (southeastern Brazil) modulated by carbonate thermodynamics, gas exchange and ecosystem metabolism during estuarine mixing. Mar. Chem. **226**: 103869. doi:10.1016/j.marchem.2020.103869

Cotovicz, L. C., Ribeiro, R. P., Régis, C. R., Bernardes, M., Sobrinho, R., Vidal, L. O., Tremmel, D., Knoppers, B. A., & Abril, G. (2021). Greenhouse gas emissions (CO2 and CH4) and inorganic carbon behavior in an urban highly polluted tropical coastal lagoon. Environ. Sci. Pollut. Res. Int. **28**: 38173–38192. doi:10.1007/s11356-021-13362-2

da Silva, A. G. A., K. Stattegger, K. Schwarzer, H. Vital, and B. Heise. 2015. The influence of climatic variations on river delta hydrodynamics and morphodynamics in the Parnaíba Delta. Brazil. J. Coast. Res. **31**: 930–940. doi:10.2112/jcoastres-d-14-00078.1

da Silva Dias, F. J., B. M. Castro, L. D. Lacerda, L. B. Miranda, and R. V. Marins. 2016. Physical characteristics and discharges of suspended particulate matter at the continent-ocean interface in an estuary located in a semiarid region in northeastern Brazil. Estuar. Coast. Shelf Sci. **180**: 258–274. doi:10.1016/j.ecss.2016.08.006

de Carvalho, A. A., A. A. Abelardo, H. P. da Silva, I. Lopes, J. E. F. de Morais, and T. G. F. da Silva. 2020. Trends of rainfall and temperature in Northeast Brazil. Rev. Bras. Eng. Agr. Amb. **24**: 15–23. doi:10.1590/1807-1929/agriambi.v24n1p15-23

Dickson, A. G., and F. J. Millero. 1987. A comparison of the equilibrium constants for the dissociation of carbonic acid in seawater media. Deep Sea Res. Part I Oceanogr. **34**: 1733–1743. doi:10.1016/0198-0149

Dickson, A. G., C. L. Sabine, and J. R. Christian. 2007. Guide to best practices for ocean CO2 measurements. *In* A. G. Dickson, C. L. Sabine, and J. R. Christian [eds.], PICES special publication. North Pacific Marine Science Organization.

dos Santos Costa, D., and M. V. J. Cutrim. 2021. Spatial and seasonal variation in physicochemical characteristics and phytoplankton in an estuary of a tropical delta system. Reg. Stud. Mar. Sci. **44**: 101746. doi:10.1016/j.rsma.2021.101746

Dürr, H. H., G. G. Laruelle, C. M. van Kempen, C. P. Slomp, M. Meybeck, and H. Middelkoop. 2011. Worldwide typology of nearshore coastal systems: Defining the estuarine filter of river inputs to the oceans. Estuar. Coasts **34**: 441–458. doi:10.1007/s12237-011-9381-y

Egleston, E. S., C. L. Sabine, and F. M. M. Morel. 2010. Revelle revisited: Buffer factors that quantify the response of ocean chemistry to changes in DIC and alkalinity. Global Biogeochem. Cycles **24**: 1–9. doi:10.1029/2008GB003407

Ferreira, T. A. B., A. G. Aquino da Silva, Y. A. Reyes Perez, K. Stattegger, and H. Vital. 2021. Evaluation of decadal shoreline changes along the Parnaíba Delta (NE Brazil) using satellite images and statistical methods. Ocean Coast Manag **202**: 105513. doi:10.1016/j.ocecoaman.2020.105513

Gattuso, J.-P., M. Frankignoulle, and R. Wollast. 1998. Carbon and carbonate metabolism in coastal aquatic ecosystems. Annu. Rev. Ecol. Syst. **29**: 405–434.

Giri, C., E. Ochieng, L. L. Tieszen, Z. Zhu, A. Singh, T. Loveland, J. Masek, and N. Duke. 2011. Status and distribution of mangrove forests of the world using earth observation satellite data. Glob. Ecol. Biogeogr. **20**: 154–159. doi:10.1111/j.1466-8238.2010.00584.x

Hamilton, S. K., S. J. Sippel, and J. M. Melack. 1995. Oxygen depletion and carbon dioxide and methane production in waters of the Pantanal wetland of Brazil. Biogeochemistry **30**: 115–141. doi:10.1007/BF00002727

IPCC, and others. 2019. Sea level rise and implications for low-Lying Islands, coasts and communities, p. 321–445. *In* H.-O. Pörtner and others [eds.], IPCC special report on the ocean and cryosphere in a changing climate. Cambridge University Press. doi:10.1017/9781009157964.006

Jeffrey, L. C., D. T. Maher, I. R. Santos, M. Call, M. J. Reading, C. Holloway, and D. R. Tait. 2018. The spatial and temporal drivers of pCO2, pCH4 and gas transfer velocity within a subtropical estuary. Estuar. Coast. Shelf Sci. **208**: 83–95.

Jeffrey, S. W. T., and G. F. Humphrey. 1975. New spectrophotometric equations for determining chlorophylls a, b, c1 and c2 in higher plants, algae and natural phytoplankton. Biochem. Physiol. Pflanzen **167**: 191–194.

Jiang, L.-Q., W.-J. Cai, and Y. Wang. 2008. A comparative study of carbon dioxide degassing in river-and marine-dominated estuaries. Limnol. Oceanogr. **53**: 2603–2615.

Joesoef, A., W. J. Huang, Y. Gao, and W. J. Cai. 2015. Air-water fluxes and sources of carbon dioxide in the Delaware estuary: Spatial and seasonal variability. Biogeosciences **12**: 6085–6101. doi:10.5194/bg-12-6085-2015

Lacerda, L. D. 2018. Burial of mangroves by mobile dunes: A climate change threat in semiarid coasts. ISME/GLOMIS Electron. J. **16**: 6–10.

Laruelle, G. G., H. H. Dürr, R. Lauerwald, J. Hartmann, C. P. Slomp, N. Goossens, and P. A. G. Regnier. 2013. Global multi-scale segmentation of continental and coastal waters from the watersheds to the continental margins. Hydrol. Earth Syst. Sci. **17**: 2029–2051. doi:10.5194/hess-17-2029-2013

Latrubesse, E. M., J. C. Stevaux, and R. Sinha. 2005. Tropical rivers. Geomorphology **70**: 187–206. doi:10.1016/j.geomorph.2005.02.005

Lee, K., T.-W. Kim, R. H. Byrne, F. J. Millero, R. A. Feely, and Y.-M. Liu. 2010. The universal ratio of boron to chlorinity

for the North Pacific and North Atlantic oceans. Geochim. Cosmochim. Acta **74**: 1801–1811. doi:10.1016/J.GCA.2009.12.027

Leopold, A., C. Marchand, J. Deborde, and M. Allenbach. 2017. Water biogeochemistry of a mangrove-dominated estuary under a semi-arid climate (New Caledonia). Springer. doi:10.1007/s12237-016-0179-9

Lewis, E., and D. Wallace. 1998. Program developed for CO2 system calculations ORNL/CDIAC-105. Carbon Dioxide Information Analysis Centre. doi:10.2172/639712

Magris, R. A., and R. Barreto. 2010. Mapping and assessment of protection of mangrove habitats in Brazil. PANAMJAS **5**: 546–556.

Maher, D. T., K. Cowley, I. R. Santos, P. Macklin, and B. D. Eyre. 2015. Methane and carbon dioxide dynamics in a subtropical estuary over a diel cycle: Insights from automated in situ radioactive and stable isotope measurements. Mar. Chem. **168**: 69–79. doi:10.1016/j.marchem.2014.10.017

Maier, M.-S., C. R. Teodoru, and B. Wehrli. 2021. Spatio-temporal variations in lateral and atmospheric carbon fluxes from the Danube Delta. Biogeosciences **18**: 1417–1437. doi:10.5194/bg-18-1417-2021

Marins, R., A. Carvalho, A. Da Silva, and M. Cavalcante. 2023. Avaliação de métodos diretos e indiretos de medição da pco2 em ambientes estuarinos. Quím. Nova **46**: 582–590. doi:10.21577/0100-4042.20230048

McLusky, D. S., and E. Wolanski. 2011. Treatise on Estuarine and Coastal Science. Elsevier.

Mehrbach, C., C. H. Culberson, J. E. Hawley, and R. M. Pytkowicx. 1973. Measurement of the apparent dissociation constants of carbonic acid in seawater at atmospheric pressure. Limnol. Oceanogr. **18**: 897–907. doi:10.4319/lo.1973.18.6.0897

Middelburg, J. J., K. Soetaert, and M. Hagens. 2020. Ocean alkalinity, buffering, and biogeochemical processes. Rev. Geophys. **58**: 1-28. doi:10.1029/2019RG000681

MMA. 2006. Caderno da RegiãoHidrográfica do Parnaíba, p. 184. *In* Ministério do Meio Ambiente, Secretaria de Recursos Hídiricos.

Maher, D. T., M. Call, I. R. Santos, and C. J. Sanders. 2018. Beyond burial: Lateral exchange is a significant atmospheric carbons ink in mangrove forests. Biol. Lett. **14**: 20180200. doi:10.1098/rsbl.2018.0200

Orr, J. C., J.-M. Epitalon, A. G. Dickson, and J.-P. Gattuso. 2018. Routine uncertainty propagation for the marine carbon dioxide system. Mar. Chem. **207**: 84–107. doi:10.1016/j.marchem.2018.10.006

Ovalle, A. R. C., C. E. Rezende, L. D. Lacerda, and C. A. R. Silva. 1990. Factors affecting the hydrochemistry of a mangrove tidal creek, Sepetiba Bay, Brazil. Estuar. Coast. Shelf Sci. **31**: 639–650. doi:10.1016/0272-7714

Paula Filho, F. J., R. V. Marins, L. Chicharo, R. B. Souza, G. V. Santos, and E. M. A. Braz. 2020. Evaluation of water quality and trophic state in the Parnaíba River Delta, Northeast Brazil. Region. Stud. Mar. Sci. **34**: 101025. doi:10.1016/j.rsma.2019.101025

Pierrot, D., and others. 2009. Recommendations for autonomous underway pCO2 measuring systems and data-reduction routines. Deep Sea Res, Part II Top. Stud. Oceanogr. **56**: 512–522.

Raymond, P. A., and J. J. Cole. 2001. Gas exchange in rivers and estuaries: Choosing a gas transfer velocity. Estuar. Coasts **24**: 312–317.

Regnier, P., and others. 2013. Anthropogenic perturbation of the carbon fluxes from land to ocean. Nat. Geosci. **6**: 597–607.

Reithmaier, G., S. G. Johnston, and D. T. Maher. 2020. Mangroves as a source of alkalinity and dissolved carbon to the coastal ocean: A case study from the Everglades National Park, Florida. JGR Biogeosci. **125**: e2020JG005812. doi:10.1029/2020JG005812

Rosentreter, J. A., D. T. Maher, D. V. Erler, R. Murray, and B. D. Eyre. 2018*a*. Seasonal and temporal CO2 dynamics in three tropical mangrove creeks–A revision of global mangrove CO2 emissions. Geochim. Cosmochim. Acta **222**: 729–745. doi:10.1016/J.GCA.2017.11.026

Rosentreter, J. A., D. T. Maher, D. V. Erler, R. Murray, and B. D. Eyre. 2018*b*. Factors controlling seasonal CO2 and CH4 emissions in three tropical mangrove-dominated estuaries in Australia. Estuar. Coast. Shelf Sci. **215**: 69–82. doi:10.1016/j.ecss.2018.10.003

Santos, I. R., and others. 2021. The renaissance of Odum's outwelling hypothesis in "blue carbon" science. Estuar. Coast. Shelf Sci. **255**: 107361. doi:10.1016/j.ecss.2021.107361

Sarma, V. V. S. S., and others. 2011. High CO2 emissions from the tropical Godavari estuary (India) associated with monsoon river discharges. Geophys. Res. Lett. **38**: 1-4. doi:10.1029/2011GL046928

Sarma, V., and others. 2012. Carbon dioxide emissions from Indian monsoonal estuaries. Geophys. Res. Lett. **39**: 1–5. doi:10.1029/2011GL050709

Sippo, J. Z., D. T. Maher, D. R. Tait, C. Holloway, and I. R. Santos. 2016. Are mangroves drivers or buffers of coastal acidification? Glob. Biogeochem. Cycles **30**: 753–766. doi:10.1002/2015GB005324

Smith, F. S., H. Vital, A. G. Aquino da Silva, K. Stattegger, and Y. A. Reyes Perez. 2021. Late Holocene evolution of the Parnaíba River Delta (Brazilian equatorial margin): Evidence of lobe switching process from mineralogical analysis and age dating on sediment cores. J. South Am. Earth Sci. **112**: 103530. doi:10.1016/j.jsames.2021.103530

Soares, M. O., and others. 2021. Challenges and perspectives for the Brazilian semi-arid coast under global environmental changes. Perspect. Ecol. Conserv. **19**: 267–278. doi:10.1016/j.pecon.2021.06.001

Stieglitz, T. C., J. F. Clark, and G. J. Hancock. 2013. The mangrove pump: The tidal flushing of animal burrows in a

tropical mangrove forest determined from radionuclide budgets. Geochim. Cosmochim. Acta **102**: 12–22. doi:10.1016/j.gca.2012.10.033

Takahashi, T., and others. 2002. Global Sea-air CO2 flux based on climatological surface ocean pCO2, and seasonal biological and temperature effects. Deep Sea Res. Part II Top. Stud. Oceanogr. **49**: 1601–1622.

Wanninkhof, R. 2014. Relationship between wind speed and gas exchange over the ocean revisited. Limnol. Oceanogr. Methods **12**: 351–362. doi:10.4319/lom.2014.12.351

Weiss, R. 1974. Carbon dioxide in water and seawater: The solubility of a non-ideal gas. Mar. Chem. **2**: 203–215.

Weiss, R. F., and B. A. Price. 1980. Nitrous oxide solubility in water and seawater. Mar. Chem. **8**: 347–359.

Yao, H., and X. Hu. 2017. Responses of carbonate system and CO2 flux to extended drought and intense flooding in a semiarid subtropical estuary. Limnol. Oceanogr. **62**: S112–S130. doi:10.1002/lno.10646

Acknowledgment

The authors thank the financial support from the Fundação Cearense de Apoio ao Desenvolvimento Científico e Tecnológico (FUNCAP) Project PR2-0101-00052.01.00/15 coordinated by RVM. LCC Jr thanks (FUNCAP; Proc. No. INT-00159-00009.01.00/19 and FUNCAP PV2-00125-00405.01.00/21) for a Visiting Professor Grant at the Marine Sciences Institute (LABOMAR/UFC) and German Federal Ministry of Education and Research through the Project Carbostore, grant no. 03F0875B, for the Postdoctoral Fellowship Grant.

Conflict of Interest

The authors have no conflict of interest to declare.

Submitted 09 March 2023
Revised 04 September 2023
Accepted 13 November 2023

Associate editor: Oscar Serrano